Available online at www.sciencedirect.com
SCIENCE DIRECT®
Journal of Hydrology 280 (2003) 105–123
Journal of Hydrology
www.elsevier.com/locate/jhydrol

Scaling effects on modeled surface energy-balance components using the NOAH-OSU land surface model

V. Sridhar[a,*], Ronald L. Elliott[b], Fei Chen[c]

[a]*Department of Civil and Environmental Engineering, University of Washington, Seattle, WA 98195-2700, USA*
[b]*Department of Biosystems and Agricultural Engineering, Oklahoma State University, Stillwater, OK 74078-6016, USA*
[c]*National Center for Atmospheric Research, Boulder, CO 80307-3000, USA*

Received 27 September 2001; revised 15 May 2003; accepted 23 May 2003

Abstract

As surface exchange processes are highly non-linear and heterogeneous in space and time, it is important to know the appropriate scale for the reasonable prediction of these exchange processes. For example, the explicit representation of surface variability has been vital in predicting mesoscale weather events such as late-afternoon thunderstorms initiated by latent heat exchanges in mid-latitude regions of the continental United States. This study was undertaken to examine the effects of different spatial scales of input data on modeled fluxes, so as to better understand the resolution needed for accurate modeling. A statistical procedure was followed to select two cells from the Southern Great Plains 1997 hydrology experiment region, each 20 km × 20 km, representing the most homogeneous and the most heterogeneous surface conditions (based on soil and vegetation) within the study region. The NOAH-OSU (Oregon State University) Land Surface Model (LSM) was employed to estimate surface energy fluxes. Three scales of study (200 m, 2 and 20 km) were considered in order to investigate the impacts of the aggregation of input data, especially soil and vegetation inputs, on the model output. Model results of net radiation and latent, sensible and ground heat fluxes were compared for the three scales. For the heterogeneous area, the model output at the 20-km resolution showed some differences when compared with the 200-m and 2-km resolutions. This was more pronounced in latent heat (12% decrease), sensible heat (22% increase), and ground heat flux (44% increase) estimation than in net radiation. The scaling effects were much less for the relatively homogeneous land area with 5% increase in sensible heat and 4% decrease in ground heat flux estimation. All of the model outputs for the 2- and 20-km resolutions were in close agreement. The results suggested that, for this study region, soils and vegetation input resolution of about 2 km should be chosen for realistic modeling of surface exchange processes. This resolution was sufficient to capture the effects of sub-grid scale heterogeneity, while avoiding the data and computational difficulties associated with higher spatial resolutions.

Keywords: Scaling; Land surface hydrology; Surface energy balance; Spatial variability; NOAH land surface model

1. Introduction

Realistic modeling of land-atmosphere interaction over a large area is advanced by the realization that the land-atmosphere exchange phenomena should be

* Corresponding author. Tel.: +1-206-685-3202; fax: +1-206-685-3836.
E-mail address: sridhar@hydro.washington.edu (V. Sridhar).

0022-1694/03/$ - see front matter © 2003 Elsevier B.V. All rights reserved.
doi:10.1016/S0022-1694(03)00220-8

addressed from both hydrological and atmospheric science perspectives. Atmospheric and soil-vegetation systems are dynamically coupled through the physical processes that produce transport of thermal energy and water mass across the land surface (Eagleson, 1978; Henderson-Sellers, 1996). The issue of global scale hydrology has reoriented the attention of hydrologists to consider the atmosphere and the land surface as an interactively coupled system (Eagleson, 1986). Studies show that the complex land-atmosphere models often contain overly simplified parameterizations of land surface hydrology, thereby resulting in inaccurate representations (Wood et al., 1992; Sivapalan and Woods, 1995). Scale interaction has emerged as one of the crucial problems for the parameterization of general circulation models (GCMs) due to the strong interconnection between land and atmospheric processes. For instance, an irrigated strip of cropland could contribute to mesoscale thunderstorm phenomena over mid-latitude regions of the Central US during a typical summer day. In order to address this issue, the understanding of the scaling properties of water and energy fluxes with their corresponding storage term (soil moisture) becomes significant (Wood, 1994).

Soil moisture and evapotranspiration are often assumed to have lesser significance and some land surface modelers fail to consider soil moisture and its related processes (e.g. exchange of surface fluxes, infiltration, sub-surface drainage) within their models as physically based, and instead parameterize soil moisture as an index to be used for evapotranspiration and runoff calculations rather than recognize it as the representative of the actual mass of moisture in the soil (Robock et al., 1998). Evapotranspiration and runoff may not be sufficiently dependent upon the soil moisture even in the simple monthly water balance simulation of land surface models (LSM) (Koster and Milly, 1997). Hence when these results are linked to GCMs, the corresponding model responses can be inaccurate even up to 20–40% depending upon the process that is in focus.

To date, understanding the effects of land surface heterogeneity at the sub-GCM grid scale level is an unfinished task. Traditionally the lumped model concept, where the spatially variable inputs and parameters are assumed to be homogeneous, has been widely used in many large-scale water balance studies. But the accuracy of the model response is dominated by sub-grid scale parameterizations of inputs and parameters (Avissar and Pielke, 1989; Hu and Islam, 1997). If the model is process based, and if the resolution of the model grid is increased, some of these modeling problems can be addressed successfully. This would probably be the most accurate approach but not always practical due to limitations in computing and data availability. However, with the advent of high-speed computers (e.g. parallel processing capabilities), the problem of voluminous data handling and processing can be overcome whereas the availability of measurements is often still a problem. In order to model spatially variable water and energy balance processes accurately, it is, therefore, necessary to understand the implications of sub-grid scale heterogeneity and its impact on model results.

This investigation is aimed at highlighting the relationship between the resolution at which surface features are represented and the accuracy in predicting fluxes. This inherent trade-off has important implications in terms of time, effort, and resources directed at activities ranging from data collection to real-time weather forecasting to long-term climate diagnostics.

The overall objective of this study is to examine the effects of different spatial scales of input data, i.e. 200 m, 2 and 20 km on modeled fluxes, and thereby better understand the resolution needed to model land surface fluxes accurately. The factor of 10 increase for each spatial scale was primarily chosen to represent the scales that might be of interest for current and (especially) future operational weather modeling. Also, the coarser scale (20 km) considered in this study should eventually be relevant to global climate modeling, as GCM grid cells continue to decrease in size. In this study, we evaluate the effects of parameterization of land surface heterogeneity on the quantification of surface energy-balance components (namely net radiation and latent, sensible and ground heat fluxes) by a distributed modeling approach. The Oregon State University Land Surface Model (hereafter referred to as 'NOAH-OSU LSM' or 'NOAH LSM') is employed to carry out this exercise. The NOAH LSM model has been coupled to the Penn State University/Mesoscale Model 5 (PSU/MM5) and an extensive validation of this model over varieties of point sites in Oklahoma provided the basis for this study (Sridhar et al., 2002).

2. Background

Typical hydrological modeling spatial scales (Dooge, 1982, 1986) are: local scale (1 m), hillslope (reach) scale (100 m), catchment scale (10 km) and regional scale (1000 km). Typical hydrological time scales are: event scale (1 day), seasonal scale (1 yr) and the long-term scale (100 yr). Models and theories developed in Darcian scale (point scale) may be applied to larger scale predictions and similarly large-area models and data are used for small-area predictions by means of parameterization. However, a major complication in parameter specification is the fact that these parameters vary from point to point because of the spatial variability always present in nature. The distributed models address this concern, and of the merits of distributed models usually claimed is that the parameters have some physical relevance and hence they should be measurable in the field. Jensen and Mantoglou (1992) believe that a theoretically justified model would provide more confident predictions, and therefore, the incentive to use physically-based models would increase in the future. On the other hand Meentemeyer (1989) indicated that minute details pertaining to reductionist sciences could be irrelevant in broad scale modeling. Another perspective is that a model that is suitable at a plot scale cannot be used to simulate a region if the simulator does not represent all relevant phenomena existing at the larger scale (Luxmoore et al., 1991).

Representing the exchanges among soil, vegetation and atmosphere at larger scales is extremely difficult due to the problems of spatial heterogeneity. Thus the question of extrapolation of non-linear hydrological processes to large scales remains largely unanswered. As scaling embodies such concepts as process descriptions, cartographic considerations or pattern analysis, and spatial and temporal variability, simple integration or aggregation of values at one level to achieve estimates at a more encompassing level of consideration may not be acceptable (DeCoursey, 1996). Dooge (1986) suggested two plausible ways of modeling catchment behavior either by fully taking into account spatial variability or by deriving models on the catchment scale in which the global effect of these spatially variable properties is parameterized in some way.

Numerous studies have shown that upscaled hydrologic equations preserve heterogeneity at field scales (Chen et al., 1994a,b; Kavvas and Karakas, 1996) and thus can be applied successfully for regional scale land surface simulations (Kavvas et al., 1998). From the perspectives of the temporal scale, a phenomenon termed 'coarse-graining in hydrological observations' occurs with the transformation of a non-stationary hydrological process at a finer scale to a stationary hydrologic process at a larger scale (Kavvas, 1999). Although some physically-based process related information could be lost, a simple expression that includes sub-grid scale heterogeneity for large scales could be used successfully (Kavvas, 1999).

In the last decade, model development has progressed to better reflect the aforementioned scale issues and the feedback mechanisms between the land and the atmosphere. For example, instead of prescribing land surface processes as boundary conditions in climate forecasting models, they are often allowed to evolve continuously at regional, continental and global scales. Further progress is needed in quantifying the accuracy of upscaled or downscaled climate/-hydrological modeling and in interpreting resultant model results for various applications including short-term weather prediction, long-term climate forecasting, water resources planning and management, and air quality monitoring.

3. Land surface model

The development of several LSMs to simulate the hydrologic processes resulted in better understanding of the various linkages that govern biosphere-atmosphere interrelationships. Each of these models has distinct features with respect to model physics, parameters (including distributed or lumped), time step, extent of testing and validation, and number of users. This study used the NOAH-OSU (Oregon State University) Land Surface Model, which has been widely recognized by the land-surface research community and which is coupled to the PSU/MM5 mesoscale model. Detailed descriptions of the NOAH-LSM model formulations and development are provided elsewhere (Chen and Dudhia, 2001; Koren et al., 1999) while a brief description is

provided below. The original LSM developed by Pan and Mahrt (1987) was modified by Chen et al. (1996) to incorporate an explicit canopy resistance formulation used by Jacquemin and Noilhan (1990). Originally, the LSM incorporated the diurnally dependent Penman potential evaporation approach of Mahrt and Ek (1984), the multi-layer soil model of Mahrt and Pan (1984) and the primitive canopy model of Pan and Mahrt (1987). Later the NCEP/Office of Hydrology/NESDIS Office of Research and Applications extended a series of improvements to refine the LSM for use in NCEP operational weather and climate prediction models. The LSM also included a physically based parameterization of frozen soil that was formulated and subsequently tested by Koren et al. (1999) against the data collected in the Rosemount site in Minnesota. The results demonstrated that the simulated soil temperature and unfrozen water content agreed with the observations reasonably well at different soil layers.

The energy balance in the model is formulated as shown in Eq. (1). Net radiation (as the 'source' term in the energy balance) is directed into latent, sensible and ground heat fluxes:

$$R_n = \mathrm{LH} + \mathrm{SH} + \mathrm{GH} \quad (1)$$

Each of these surface energy-balance components is computed using physically-based formulations. The four-level soil layer configuration (with thicknesses of 0.1, 0.3, 0.6 and 1.0 m) is adopted in the LSM for capturing the daily, weekly and seasonal evolution of soil moisture and mitigating the possible truncation error in discretization. The LSM can accommodate one canopy layer and its total depth of soil layers is 2 m. The lower 1 m acts as a reservoir with gravity drainage at the bottom, and the upper 1 m of soil serves as the root zone depth. The surface skin temperature is determined following Mahrt and Ek (1984) by applying a single linearized surface energy balance equation representing the combined ground/vegetation surface. The LSM simulation of seasonal and diurnal variation in evaporation, soil moisture, sensible heat flux and surface skin temperature agrees well with field observations and its performance appears to be better than many LSMs (Chen et al., 1996). Various studies (Betts et al., 1997; Chen et al., 1997; Yucel et al., 1998) showed that the coupled Eta/OSULSM system indeed improved the short-range prediction of surface heat fluxes, near-surface sensible variables, planetary boundary layer and precipitation. Marshall (1998) studied the performance of this LSM in an uncoupled mode for Oklahoma conditions and found that the model overestimated net radiation and underestimated ground heat flux. The model demonstrated that excess energy predicted was predominantly assigned to the computation of latent heat flux as opposed to sensible heat flux as reported by Sridhar et al. (2002) through a validation study using Oklahoma Atmospheric Surface-layer Instrumentation System (OASIS) measurements. As the model is used here in an uncoupled fashion, the model input includes soil and vegetation types and meteorological forcing variables. Prognostic variables include soil moisture and temperature in the soil layers, water intercepted on the canopy and snow accumulated on the ground. Model simulations also provide estimates of surface energy balance components (net radiation and latent, sensible, and ground heat fluxes).

4. Study area and data

4.1. Study area description

This research utilized the study area for the Southern Great Plains, 1997 (SGP97) Hydrology Experiment (Fig. 1). SGP97 focused on the central section of Oklahoma from Comanche and Stephens counties in the south to Grant and Kay counties in the north, covering a soil moisture mapping area of about 50 km × 280 km (SGP97 Hydrology Experimental Plan 1997; Jackson et al., 1999). SGP97 took advantage of the availability of the Oklahoma Mesonet (Elliott et al., 1994; Brock et al., 1995), and was built upon the success of the Little Washita 1992 experiment (Rodriguez-Iturbe et al., 1996) in demonstrating the viability of L-band radiometry for remotely sensing surface moisture. The main objective of SGP97 was to understand soil moisture dynamics in space and time using remotely sensed and field measurements.

4.2. Soil and vegetation data

The model soil and vegetation parameters are shown in Table 1. The Geographic Information

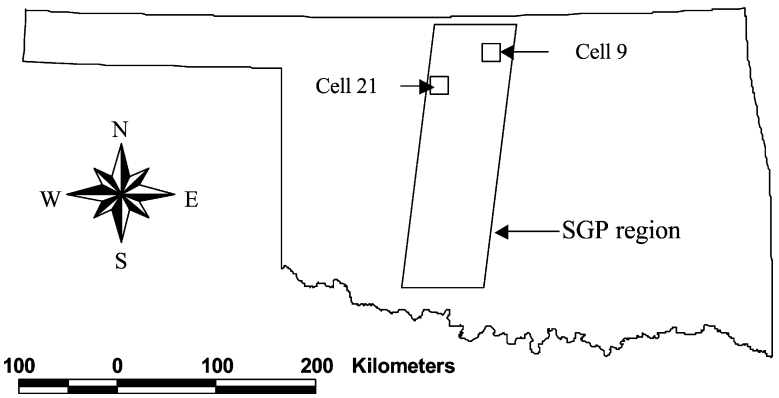

Fig. 1. Schematic map of Southern Great Plains 1997 (SGP97) and the study area.

Systems (GIS) soil data for this study was available from the Map Information Analysis and Display System (MIADS) of the USDA Natural Resources Conservation Service. Soil surveys conducted for the individual counties had been merged to create a seamless statewide data set in gridded format. The resolution of the MIADS soil data was 200 m (4 ha) and hence the finest resolution of this study is 200 m.

Land use class information, derived from Landsat Thematic Mapper (TM) data, was available for the SGP97 study area that included the period of June–July 1997. These 30-m resolution land use data were aggregated using a majority filter (the value that appears most often) in order to match the spatial resolution of the 200-m soil data. If no majority value existed, the neighborhood parameters could be changed to include more grid cells. However, that situation did not arise in this case.

The Conterminous US Advanced Very High Resolution Radiometer (AVHRR) satellite data provided measurements of Normalized Difference Vegetation Index (NDVI) with a 1-km resolution. A time series of biweekly composite NDVI data sets was obtained from the USGS EROS Data Center.

4.3. Weather data

The Oklahoma Mesonet, an automated network of 114 stations (Elliott et al., 1994; Brock et al., 1995) provided meteorological data. The Mesonet sites used for this study included LAHO (Lat: 36° 23′ 3″ N, Long: 98° 6′ 41″ W, elev: 395 m) and MEDF (lat:36° 47′ 31″ N, long: 97° 44′ 44″ W, elev: 330 m). These sites were assigned to Cell 21 and Cell 9, respectively, based on the nearest neighbor approach (description of these study cells will follow in Section 4.4). The data from the Oklahoma Mesonet consisted of 5-min averages, which were then averaged over 1-hour intervals. The variables used were air temperature (K), specific humidity ($kg\,kg^{-1}$), wind speed ($m\,s^{-1}$), pressure (Pa), precipitation ($kg\,m^{-2}\,s^{-1}$) and solar radiation ($W\,m^{-2}$). It should be noted that air temperature in K and specific humidity were derived quantities using the original Mesonet variables. Longwave downwelling radiation was estimated using the scheme discussed in Sridhar and Elliott (2002). This longwave radiation scheme uses near-surface vapor pressure and air temperature data.

Table 1
List of vegetation and soil parameters used in the LSM

Vegetation parameters	Soil parameters
Albedo	Porosity
Roughness length	Air dry soil moisture content
Shade factor	Saturation soil suction
Root depth	Saturation soil conductivity/diffusivity
Minimum stomatal resistance	Soil conductivity/diffusivity coefficient
A parameter in the radiation stress function	Field capacity
A parameter in the vapor pressure deficit function	Wilting point
	Soil quartz content

4.4. Identification of the homogeneous and the heterogeneous cell

Due to the difficulties associated with handling and processing the huge volume of 200-m resolution data, a representative subset of the SGP97 study area was selected for the scaling analysis. A simple statistical analysis of the combined soil and land use data was performed to identify the most homogeneous and the most heterogeneous 20-km cells within the SGP97 area. Seventy cells, each 20 km × 20 km, were analyzed using FRAGSTATS (McGarigal and Marks, 1995).

Landscape indices were computed to find the fragmentation as shown in Table 2. A total of 9 soil classes and 13 land-use classes were present in the 28,000 km^2 area. 'Patches' in the landscape represent homogeneous, discrete areas, with the smallest area being 4 ha in this study. The indices considered in the analysis included the number of patches, the largest patch index (the area of the largest patch in the landscape divided by total landscape area), patch density (number of patches in the landscape divided by total landscape area), diversity index (sum of the proportional abundance of each patch type multiplied by that proportion; it increases as the number of different patch types increases), evenness index (sum of the proportional abundance of each patch type multiplied by that proportion divided by the logarithm of the number of patch types), interspersion/juxtaposition index (the observed interspersion over the maximum possible interspersion for the given number of patch types), and the contagion index (observed contagion over the maximum possible contagion for the given number of patch types).

Table 2
Landscape indices for the heterogeneous cell (#21) and the homogeneous cell (#9)

Landscape indices	Cell 21	Cell 9
Number of patches	2455	1414
Largest patch index (%)	3.76	27.33
Patch density (#/100 ha)	6.51	3.6
Shannon's diversity index	3.28	1.94
Simpson's diversity index	0.94	0.69
Modified Simpson's diversity index	2.78	1.18
Shannon's evenness index	0.73	0.46
Simpson's evenness index	0.95	0.7
Modified Simpson's evenness index	0.62	0.28
Interspersion/juxtaposition index (%)	65.58	50.49
Contagion index (%)	39.57	61.06

The fragmentation analysis of the various indices led to the identification of Cell 21 as the most heterogeneous and Cell 9 as the most homogeneous of the 70 cells. The heterogeneity for Cell 21 is explained by the largest number of patches and the high patch density. Other indices such as diversity and evenness also suggested a high variability for Cell 21. Conversely, the indices calculated for Cell 9 suggested a high degree of homogeneity. Therefore, our study focused on Cell 21 and Cell 9 for further analysis. It is important to mention that these areas were defined within the SGP97 region and do not necessarily represent the degree of heterogeneity and homogeneity that might be seen at continental or even regional scales.

Cell 21 was situated in the west-central part of SGP97 (Fig. 1) and its Universal Transverse Mercator (UTM) coordinates were (553,000, 3,998,000) and (573,000, 4,018,000) for the southwest and northeast corners, respectively. The variability in soil and land use in this 20 km × 20 km grid was high. As shown in Fig. 2a, at the 200-m resolution, Cell 21 contained 13 vegetation classes with pastureland (42%) and wheat (33%) as predominant types. The soil as shown in Fig. 3a consisted of nine different textures, the major ones being sand (23%), silt loam (18%), loamy sand (16%) and sandy loam (12%).

Cell 9 was located in the northeast part of SGP97 (Fig. 1) and its UTM coordinates were (613,000, 4,058,000) and (633,000, 4,078,000) for the southwest and northeast corners, respectively. This cell primarily consisted of wheat (59%) and pastureland (24%) as shown in Fig. 4a. Silt loam occupied 83% of the cell area with several other textures having minor presence (Fig. 5a).

4.5. Aggregation of the input data

The high-resolution data (200 m) were used to develop the input data sets for two coarser resolutions, 2 and 20 km. These scales were chosen to represent the resolution of current and future operational weather modeling efforts. With a decreasing trend in GCM cell size in recent times, the coarsest scale of this study should eventually be relevant to global

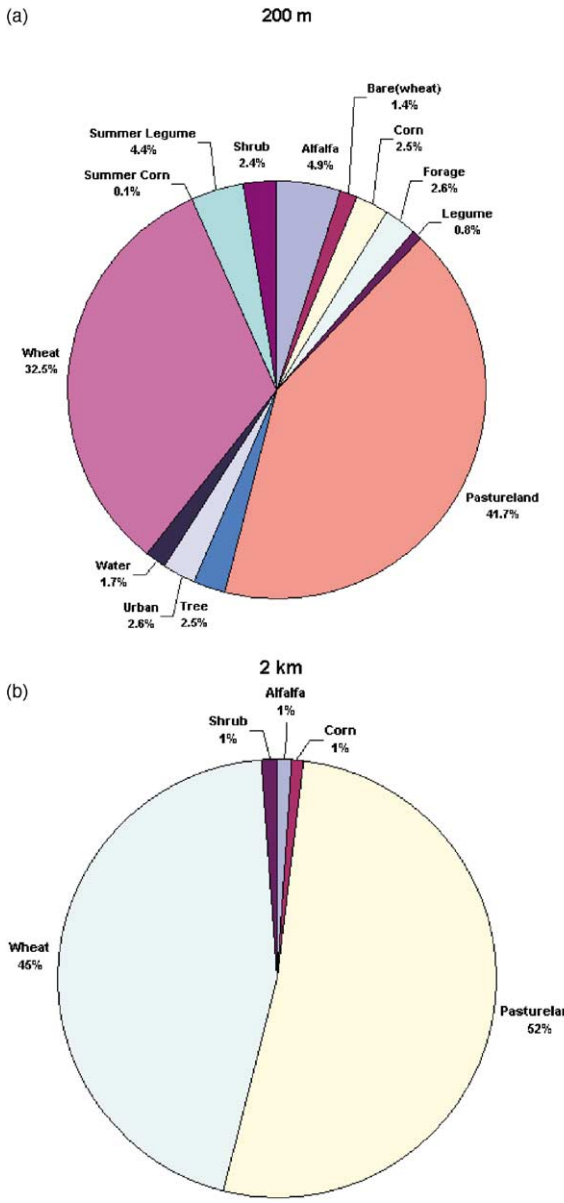

Fig. 2. (a) Land use types of the heterogeneous area (Cell 21) at 200-m resolution. (b) Land use types of the heterogeneous area (Cell 21) at 2-km resolution.

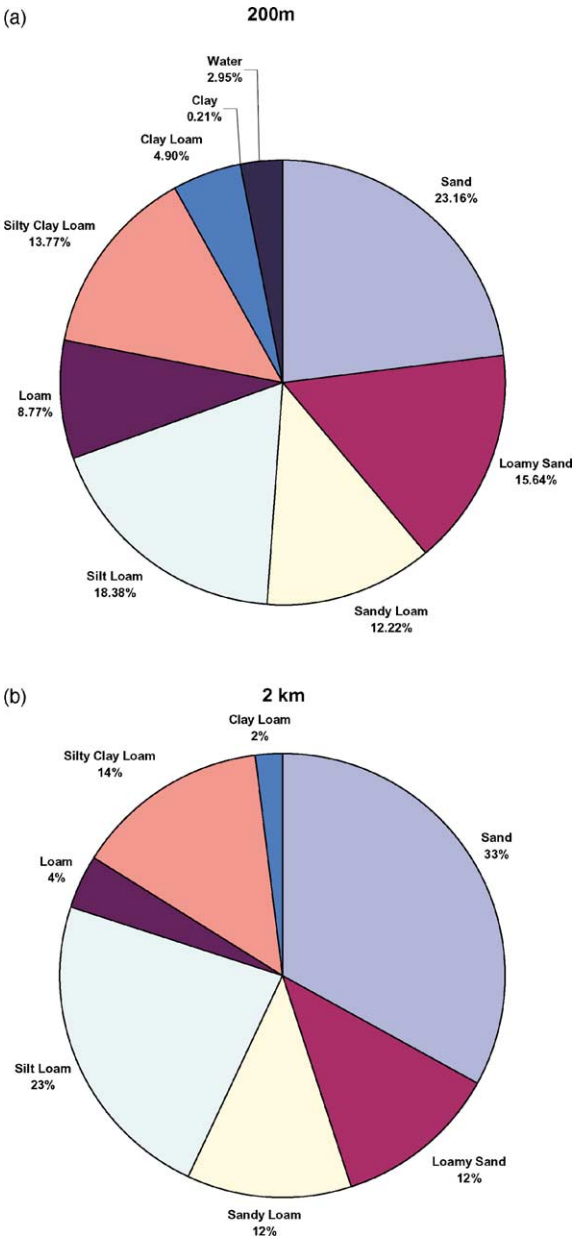

Fig. 3. (a) Soil types of the heterogeneous area (Cell 21) at 200-m resolution. (b) Soil types of the heterogeneous area (Cell 21) at 2-km resolution.

climate modeling. The soil and land use types were each aggregated using a majority filter on 100 of the 200-m cells (in the case of the 2-km resolution) and on 10,000 of the 200-m cells (in the case of the 20-km resolution). As shown in Fig. 2b, land use types for Cell 21 were reduced to five classes at the 2-km resolution as compared to 13 classes at the 200-m resolution. Similarly, Fig. 3b shows that the number of soil types was reduced from nine to seven. The difference is even more dramatic for

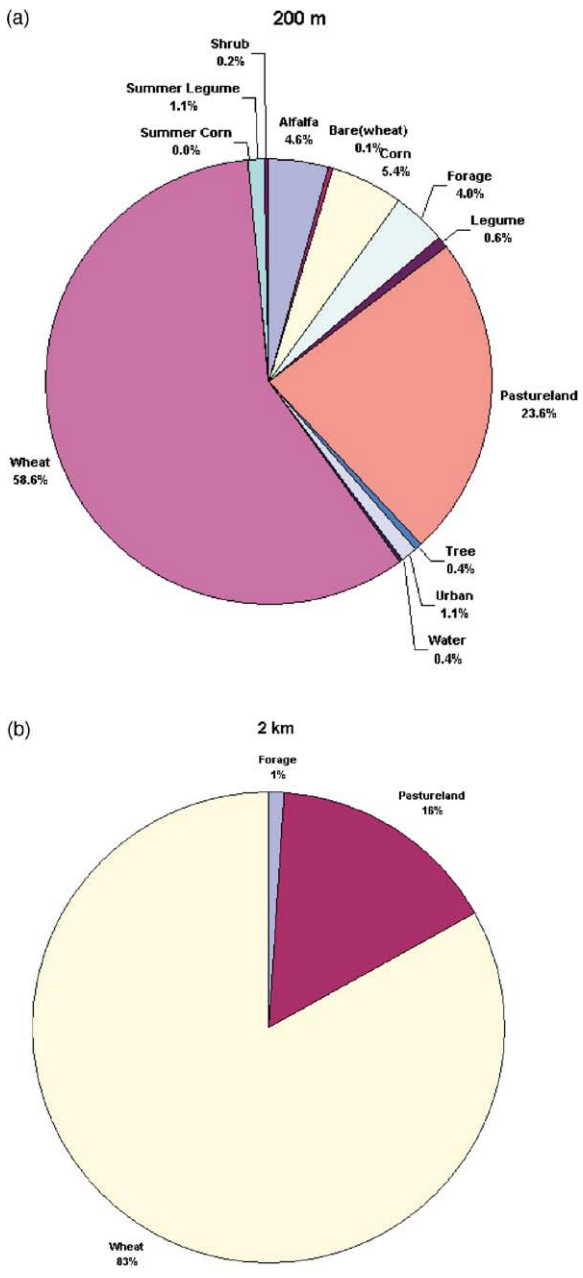

Fig. 4. (a) Land use types of the homogeneous area (Cell 9) at 200-m resolution. (4) Land use types of the homogeneous area (Cell 9) at 2-km resolution.

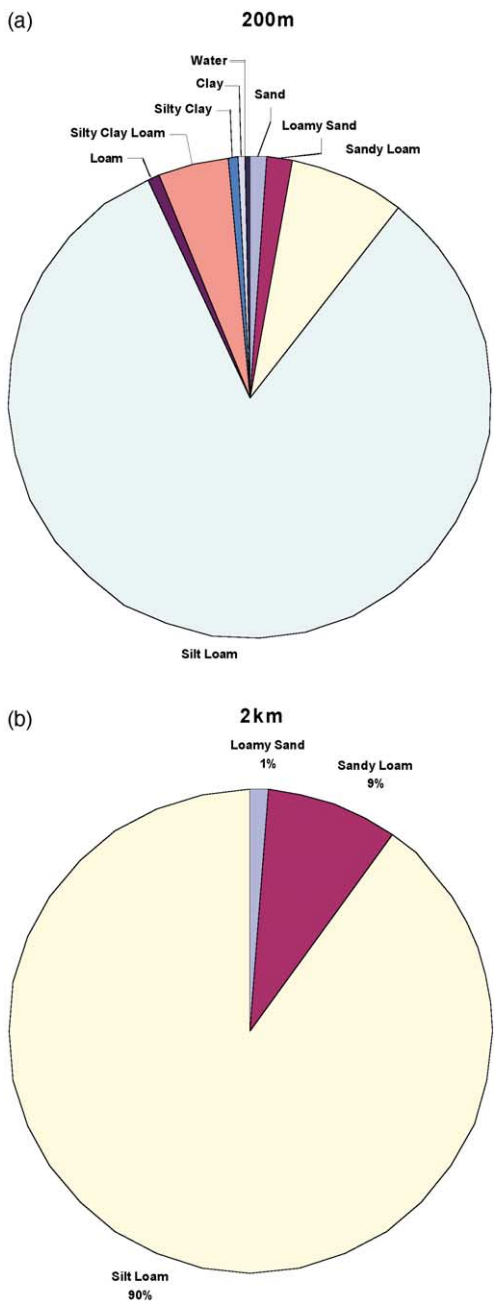

Fig. 5. (a) Soil types of the homogeneous area (Cell 9) at 200-m resolution. (b) Soil types of the homogeneous area (Cell 9) at 2-km resolution.

the homogeneous cell (Cell 9). As evident from Fig. 4b, land use at the 2-km resolution was reduced from 13 classes to only three (with 83% wheat). Similarly, only three soil types remained in Cell 9 at the 2-km resolution, with 90% silt loam (Fig. 5b). So, the clear distinction between the heterogeneous (#21) and homogeneous (#9) cells was still evident after the aggregation to 2 km.

4.6. Area-averaged and dominant-landuse-based NDVI for green vegetation fraction

The LSM requires green vegetation fraction as a key input. Two methods of computing green vegetation fraction were utilized, and the resulting simulated surface fluxes were compared. In the first approach, an 'area-averaged' NDVI was computed in Arc/Info GIS and it is simply the numerical average of the NDVI values over the given area. For instance, averages of 4 and 400 numerical values of NDVI (1-km resolution) were computed to obtain a cell-average NDVI value for 2 and 20 km, respectively. In the second approach, the NDVI value for a given area is tied to the dominant land use in that area. 'Dominant-land use-based' NDVI was computed by first applying a majority filter on 100 and 10,000 land use 'pixels' (200-m resolution) for 2 and 20 km, respectively. Then an average was taken of the NDVI values for all pixels with that majority land use. As opposed to the area-average, this approach was more likely to result in an NDVI value that is consistent with the single vegetation type assigned to a modeling area.

From both the area-averaged and dominant-land-use-based NDVI data, vegetation fraction (f_g) was computed using the Gutman and Ignatov (1998) method:

$$f_g = \frac{(\mathrm{NDVI} - \mathrm{NDVI}_{min})}{(\mathrm{NDVI}_{max} - \mathrm{NDVI}_{min})} \quad (2)$$

Bare soil NDVI (NDVI_{min}) and dense vegetation NDVI (NDVI_{max}) are defined as 0.04 and 0.52, respectively, and they correspond to seasonally and geographically invariant constants for desert and evergreen clusters. As NDVI was available from the biweekly composite images, the computed vegetation fraction based on NDVI was then linearly interpolated on a daily basis. The vegetation fractions derived based on area-averaged based NDVI and dominant-landuse-based NDVI are referred to herein as the area-averaged vegetation fraction and the dominant-land-use-based vegetation fraction, respectively.

4.7. Hydrological simulations

The model simulations were carried out over a five-month period (from 1 March 1997 to 31 July 1997). The simulation from March through May was considered as the model 'spin-up' period before the SGP97 duration of June–July. Although a longer spin-up period might be required in some modeling situations, the spring months in the Southern Great Plains tend to be characterized by significant precipitation and relatively low evaporation rates. Thus, an assumed initial soil moisture condition of field capacity, followed by a three-month period of surface forcing, was considered to provide an adequate lead-in to the June–July period. The initial soil temperatures at 5, 25, and 60 cm were assigned based on measurements from Campbell Scientific 229-L sensors located at Mesonet sites. The soil temperature at the 3-m depth was taken as the 2-year mean annual near-surface air temperature. The model was executed on an hourly time step, and the results were aggregated daily. The model was implemented for Cell 21 and Cell 9 individually for all three scales, and therefore, six different simulations were performed. Though the model was run continuously for a five-month period, due to the huge volume of output generated at the 200-m resolution, the model was coded to write the output at the 200-m resolution only for selected days. The days were chosen to fall within the SGP97 period. Nine days with relatively high solar radiation were chosen as 'clear days' (18, 25, 27, and 30 June; 3, 6, 14, 22, and 23 July), while four days with relatively low solar radiation were considered as 'cloudy days' (23 June; 11, 15, and 20 July). For the 2-km and the 20-km resolutions, simulation results were obtained throughout the study period.

5. Results and discussion

The sensitivity of the model to the two approaches of green vegetation fraction computation discussed in Section 4.6 was analyzed first by comparing the model estimated surface energy-balance components, i.e. net radiation, latent, sensible and ground heat fluxes. For both Cell 21 and Cell 9, there was virtually no difference in the model output resulting from these two vegetation fraction approaches. This was consistent for both clear and cloudy days. The differences in NDVI values for the two approaches were less than 3% and they were not large enough to cause appreciable differences in the computed vegetation

fraction. For the subsequent model runs, the dominant-landuse-based vegetation fraction was used.

5.1. Comparison of the model output for the three scales

The hourly model simulations of surface energy-balance components were aggregated on a daily basis. Then, the numerical average over the domain was computed for comparing the results across the three scales, i.e. 200 m, 2 and 20 km. The spatial representations of the model output for Cell 21 and Cell 9 for 18 June 1997 are shown in Figs. 6–9. The variability in net radiation was particularly high at the 200-m resolution for Cell 21, and for both cells, the variability was greatly reduced at the 2-km resolution (Fig. 6). A single daily average value over the 20-km domain for each of the energy-balance component is not shown in a figure but presented in Tables 3 and 4. The latent heat flux estimation demonstrated very similar trends (Fig. 7). For sensible heat flux (Fig. 8), there was again a reduction in variability as one moved to the coarser resolution, but in this case the distinction between the behavior of Cell 21 and Cell 9 was much less. The residual energy-balance component of the model, ground heat flux, clearly exhibited a greater variability in Cell 21 than in Cell 9 (Fig. 9).

Tables 3 and 4 summarize the numerical model output. Maximum, minimum and average values are shown for each study day. Referring to 18 June 1997

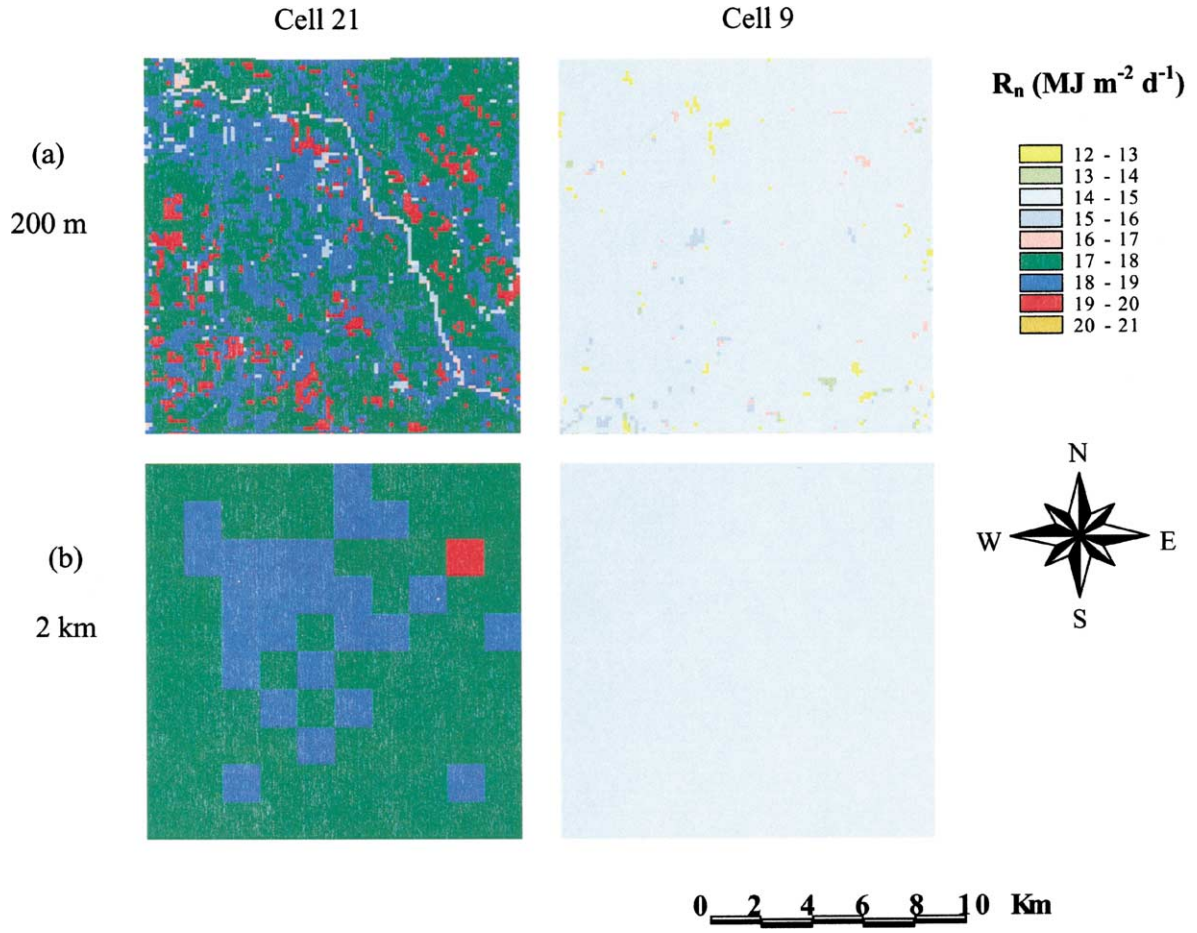

Fig. 6. Scale comparisons of modeled total daily net radiation (R_n) for the heterogeneous (Cell 21) and homogeneous area (Cell 9) for 18 June 1997.

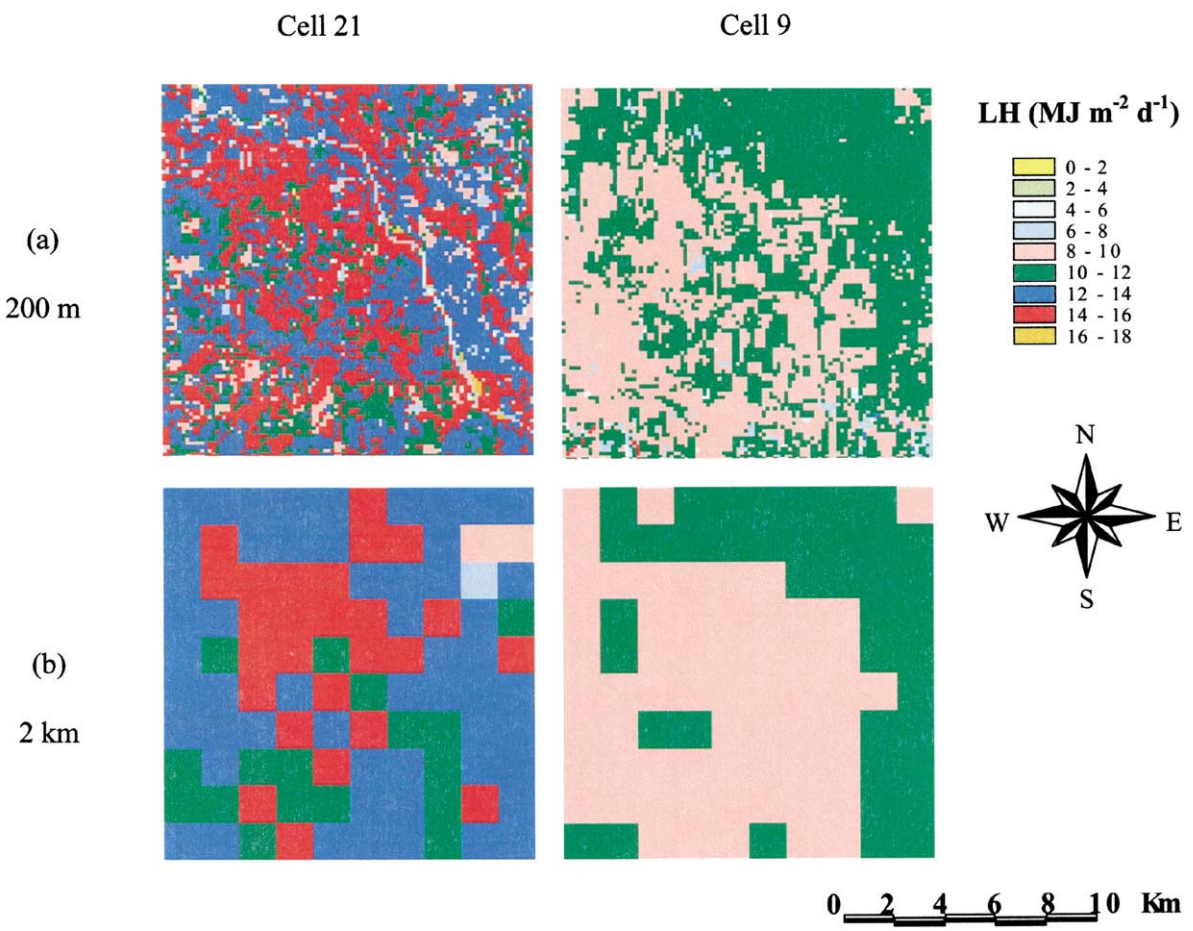

Fig. 7. Scale comparisons of modeled total daily latent heat flux (LH) for the heterogeneous (cell 21) and homogeneous area (Cell 9) for 18 June 1997.

at the 200-m resolution, the daily average net radiation was 18.39 MJ m^{-2} d^{-1} with a range of about 15–20 MJ m^{-2} d^{-1} for Cell 21, whereas for Cell 9 the average and range were 15 MJ m^{-2} d^{-1} and 12–17 MJ m^{-2} d^{-1}, respectively. Similarly, a high variability exhibited in soil and vegetation types over Cell 21 caused a higher range in estimated latent, sensible and ground heat fluxes when compared with Cell 9 wherein soil and vegetation types exhibited less variability. It was observed that the range of the cell-by-cell model output was greater at the 200-m resolution than at the 2-km resolution, for all of the simulated components. In other words, the range of the lower-resolution model output always fell within the range of the high-resolution output, indicating that the variability in the output was reduced at coarser scales. The drop in the estimation of latent heat flux over the heterogeneous area (#21) was close to 12% (200-m vs. 20-km) whereas it was only about 2.5% over the homogenous area (#9). The resultant increase in the estimation of sensible and ground heat flux for cell #21 was about 22 and 41%, respectively (by construct of the model as shown in Eq. (1)), while cell #9 exhibited an increase of 5% in sensible heat estimation and 4% decrease in the estimation of ground heat flux.

Fig. 10 shows the time series plot of all four surface energy-balance components at 200 m, and 2 km, for Cell 21. The time period is June 15–July 25. As shown in Fig. 10a, the discrete series of

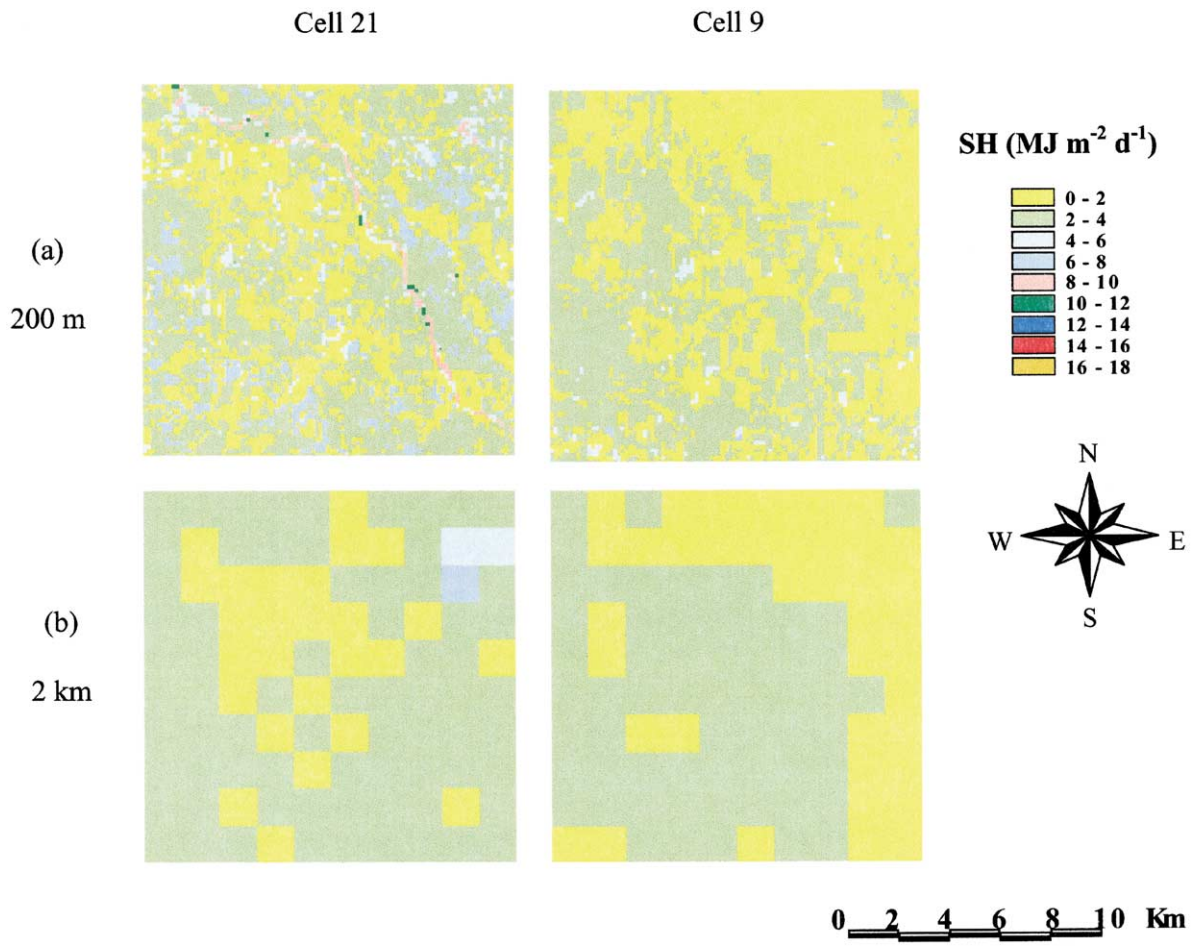

Fig. 8. Scale comparisons of modeled total daily sensible heat flux (SH) for the heterogeneous (Cell 21) and homogeneous area (Cell 9 for 18 June 1997.

domain average net radiation for 200 m (13 days) agreed very well with the continuous time series for both the 2- and 20-km resolutions. This indicated that, in spite of the aggregation of input variables from 200 m to 2 and 20 km, the model estimates of net radiation were very closely matched across these scales. This is perhaps to be expected because net radiation is dominated by the magnitude of incoming solar radiation and is only minimally influenced by vegetation and soil parameters (i.e. the albedo). It should be remembered that weather data from a single site were applied at all three scales for the entire domain of Cell 21 as the sub-grid scale weather variability within a 20-km cell was considered to be minimal. The 200-m and 2-km output for latent heat flux matched very closely while the 20-km output did show some deviations (Fig. 10b). Fig. 10c suggested that the sensible heat flux estimations at 20 km were higher than for the other two resolutions, and the magnitude of difference was similar to that for the latent heat flux estimation. Finally, the residual term in the energy budget (the ground heat flux), as shown in Fig. 10d, tended to be predicted slightly higher at the 20-km resolution than at the 200-m and 2-km resolutions. Thus, scaling effects were manifested in the partitioning of the energy, especially latent and sensible heat. These differences became evident at the 20-km scale.

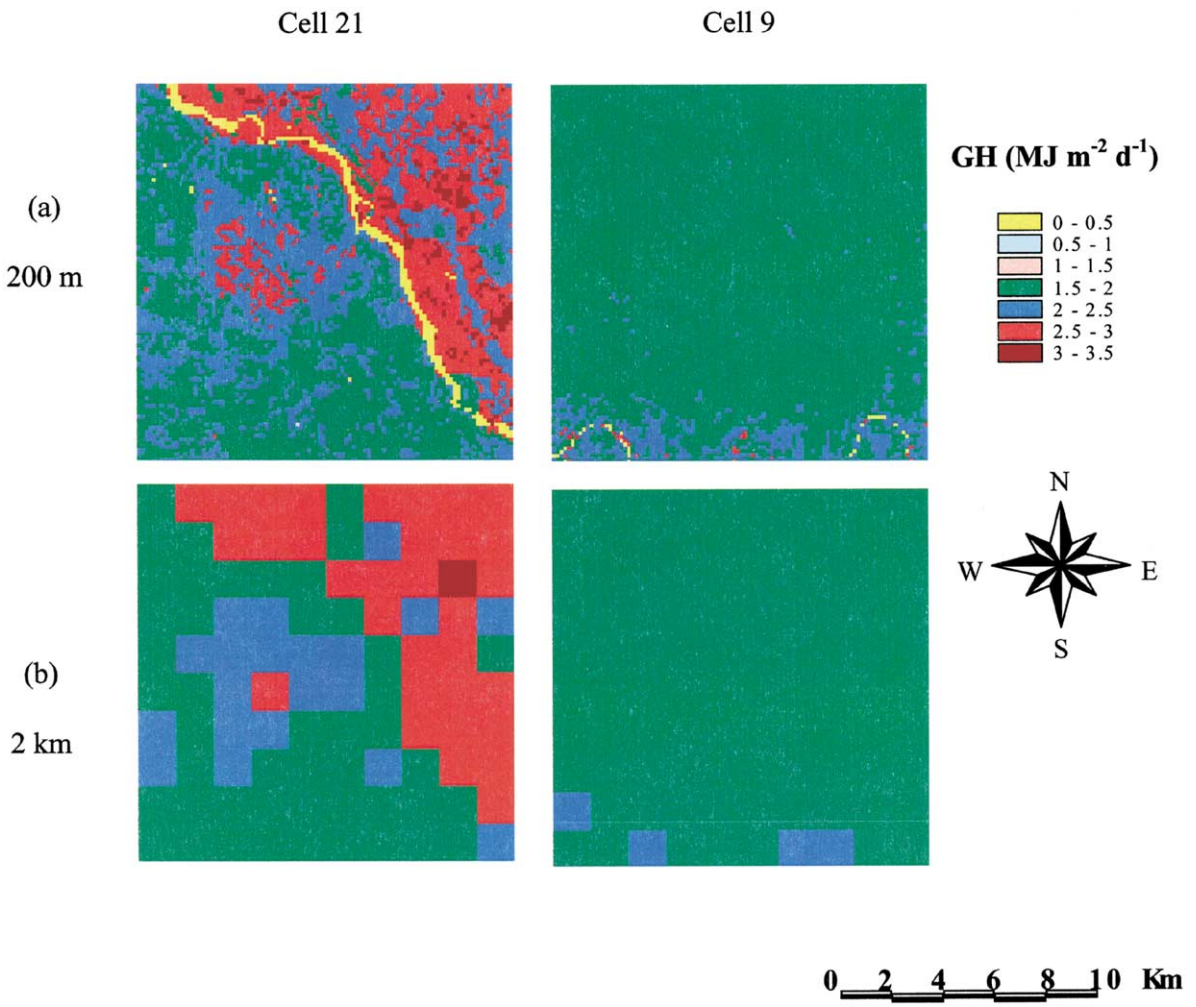

Fig. 9. Scale comparisons of modeled total daily ground heat flux (SH) for the heterogeneous (Cell 21) and homogeneous area (Cell 9 for 18 June 1997.

The modeling results for the homogeneous area (Cell 9) were studied in a similar way. Fig. 11 represents the time series plots of simulated surface energy-balance components for all three scales. The results of the simulated net radiation for 200 m, 2 and 20 km again agreed very well as shown in Fig. 11a. Both latent heat flux (Fig. 11b) and sensible heat flux (Fig. 11c) showed slight deviations at the coarsest scale, i.e. 20 km, but overall the results for the three scales agreed closely. Ground heat flux matched very well at all three scales as shown in Fig. 11d. As expected, the aggregation of input data had less impact on the model output when the variability in surface conditions was less.

5.2. Implications of the scaling results

The estimated net radiation for the heterogeneous area clearly shows that there was no bias in the estimates across the three scales. Also, the estimation of latent heat flux at 200 m and 2 km agreed very well while there was a negative bias in the estimation as the scale moved to 20 km. Sensible heat flux predictions again indicated a bias at the 20-km scale,

Table 3
Daily average modeled energy-balance components for the heterogeneous area (Cell 21) at three scales of input aggregation

Type of day	Date		R_n (MJ m^{-2} d^{-1})			LH (MJ m^{-2} d^{-1})			SH (MJ m^{-2} d^{-1})			GH (MJ m^{-2} d^{-1})		
			200 m	2 km	20 km	200 m	2 km	20 km	200 m	2 km	20 km	200 m	2 km	20 km
Clear day	18-Jun-97	MAX	20.24	19.55		17.49	15.98		16.82	7.99		3.26	3.11	
		MIN	15.10	17.76		0.33	8.46		0.91	1.06		0.05	1.70	
		AVE	18.39	18.31	18.39	13.18	13.26	12.83	3.05	2.85	2.89	2.16	2.20	2.67
	25-Jun-97	MAX	18.09	17.39		15.15	13.29		15.18	8.12		2.79	2.12	
		MIN	13.70	15.82		0.40	7.15		1.82	2.28		0.02	1.11	
		AVE	16.33	16.29	16.21	10.85	10.88	9.94	4.15	3.99	4.67	1.33	1.42	1.61
	27-Jun-97	MAX	15.79	15.19		12.67	11.85		13.47	7.25		1.27	1.13	
		MIN	11.95	13.82		0.14	6.81		2.04	2.12		0.01	0.42	
		AVE	14.28	14.21	14.22	10.01	10.07	9.42	3.56	3.41	3.73	0.72	0.73	1.07
	30-Jun-97	MAX	20.53	19.73		16.03	14.85		17.60	9.60		2.77	2.48	
		MIN	15.83	17.92		0.61	7.65		2.43	2.62		0.05	1.37	
		AVE	18.58	18.41	18.45	11.92	11.88	10.45	4.87	4.78	5.85	1.78	1.75	2.15
	03-Jul-97	MAX	20.61	19.79		16.81	15.06		17.26	10.99		1.71	1.17	
		MIN	15.65	17.74		0.62	7.37		2.36	3.68		0.00	0.27	
		AVE	18.55	18.51	18.33	11.89	11.75	9.88	6.21	6.16	7.59	0.46	0.61	0.87
	06-Jul-97	MAX	18.06	17.21		14.25	12.39		14.80	9.45		2.21	2.11	
		MIN	13.48	14.91		0.44	3.98		2.48	2.87		0.04	1.10	
		AVE	16.15	16.04	15.91	9.98	9.90	8.17	4.84	4.72	6.09	1.33	1.42	1.65
	14-Jul-97	MAX	20.24	19.29		14.85	12.93		17.08	10.16		2.54	1.96	
		MIN	15.53	17.46		0.62	7.17		3.86	4.40		0.03	0.97	
		AVE	18.11	17.96	17.77	10.43	10.26	7.96	6.44	6.49	8.47	1.23	1.21	1.33
	22-Jul-97	MAX	18.29	17.63		12.86	12.45		14.74	6.13		3.24	3.18	
		MIN	13.49	16.05		0.29	8.32		2.26	2.41		0.05	1.41	
		AVE	16.45	16.40	16.39	10.89	10.95	9.78	3.57	3.34	3.78	1.99	2.11	2.84
	23-Jul-97	MAX	18.23	17.50		13.49	13.23		14.62	6.38		3.34	2.95	
		MIN	13.29	15.94		0.37	8.17		1.57	1.83		0.04	1.40	
		AVE	16.44	16.37	16.29	11.39	11.41	9.94	3.16	2.97	3.65	1.89	1.99	2.71
Cloudy day	23-Jun-97	MAX	11.61	11.25		9.79	9.72		10.22	3.94		0.71	0.49	
		MIN	8.95	10.04		0.13	7.25		0.51	0.72		-0.12	-0.11	
		AVE	10.37	10.28	10.35	8.52	8.64	8.00	1.56	1.50	1.75	0.32	0.17	0.63
	11-Jul-97	MAX	9.62	9.26		7.89	8.31		7.95	3.17		1.30	0.91	
		MIN	7.16	8.27		0.16	5.52		0.44	0.39		-0.36	-0.18	
		AVE	8.51	8.46	8.43	6.83	6.78	5.88	1.20	1.21	1.65	0.48	0.48	0.90
	15-Jul-97	MAX	7.02	6.63		7.35	7.12		5.43	2.32		0.27	-0.26	
		MIN	5.03	5.82		0.27	4.80		-0.54	-0.27		-1.09	-0.76	
		AVE	6.07	6.06	5.91	6.04	6.01	4.89	0.64	0.59	1.41	-0.61	-0.54	-0.40
	20-Jul-97	MAX	9.03	8.76		7.39	7.56		7.09	2.04		1.97	1.93	
		MIN	6.35	7.87		0.13	4.93		0.22	-0.09		0.02	0.63	
		AVE	8.05	8.02	8.06	6.11	6.18	5.47	0.76	0.58	0.64	1.18	1.25	1.95

Table 4
Daily average modeled energy-balance components for the homogeneous area (Cell 9) at three scales of input aggregation

Type of day	Date		R_n (MJ $m^{-2}d^{-1}$)			LH (MJ m^{-2} d^{-1})			SH (MJ m^{-2} d^{-1})			GH (MJ m^{-2} d^{-1})		
			200 m	2 km	20 km	200 m	2 km	20 km	200 m	2 km	20 km	200 m	2 km	20 km
Clear day	18-Jun-97	MAX	17.00	15.36		16.25	12.19		8.79	3.29		2.87	2.24	
		MIN	12.44	14.74		3.57	9.29		0.03	1.26		0.06	1.64	
		AVE	15.01	14.91	14.85	10.78	10.54	10.30	2.44	2.60	2.75	1.80	1.78	1.80
	25-Jun-97	MAX	16.33	14.80		15.17	10.16		10.22	5.29		1.83	1.24	
		MIN	12.37	14.25		2.39	7.72		0.46	3.67		0.01	0.82	
		AVE	14.41	14.40	14.30	8.76	8.70	8.60	4.80	4.78	4.88	0.85	0.92	0.82
	27-Jun-97	MAX	19.63	17.70		16.62	13.22		10.92	5.29		2.33	1.72	
		MIN	14.80	17.10		3.86	10.58		1.62	3.25		0.03	1.01	
		AVE	17.40	17.30	17.23	11.95	11.72	11.45	4.32	4.48	4.68	1.14	1.11	1.11
	30-Jun-97	MAX	18.64	16.92		15.36	14.59		9.67	2.68		3.27	2.12	
		MIN	13.95	16.31		4.21	11.97		0.55	0.73		0.06	1.41	
		AVE	16.58	16.49	16.41	12.92	12.97	12.41	1.95	1.92	2.30	1.70	1.60	1.69
	03-Jul-97	MAX	20.37	18.55		17.60	15.35		11.16	5.64		0.84	0.42	
		MIN	15.25	17.83		4.09	12.10		1.18	3.01		-0.05	0.07	
		AVE	18.09	18.04	17.89	13.57	13.26	12.93	4.47	4.67	4.94	0.06	0.10	0.02
	06-Jul-97	MAX	19.51	17.80		15.95	13.31		10.86	5.19		2.04	1.45	
		MIN	14.76	17.14		4.26	10.91		2.26	3.31		0.03	0.95	
		AVE	17.39	17.27	17.22	11.57	11.44	11.18	4.78	4.78	5.02	1.04	1.05	1.02
	14-Jul-97	MAX	18.91	17.16		16.26	12.01		13.87	6.79		1.41	0.83	
		MIN	14.67	16.62		1.54	9.25		1.68	4.58		0.01	0.40	
		AVE	16.81	16.72	16.67	10.42	10.39	10.27	5.85	5.85	5.90	0.55	0.49	0.51
	22-Jul-97	MAX	20.18	18.48		13.75	12.89		11.66	4.95		3.48	2.47	
		MIN	15.09	17.91		3.36	11.08		3.45	3.53		0.05	1.68	
		AVE	18.11	18.02	17.96	11.69	11.53	11.33	4.62	4.66	4.84	1.80	1.83	1.78
	23-Jul-97	MAX	20.43	18.73		13.81	13.66		12.38	5.12		2.75	2.08	
		MIN	15.16	18.18		2.73	11.49		3.47	3.77		0.05	1.29	
		AVE	18.39	18.31	18.24	12.23	12.09	11.89	4.70	4.76	4.92	1.46	1.45	1.44
Cloudy day	23-Jun-97	MAX	10.46	9.18		10.03	7.97		6.90	2.46		0.17	-0.18	
		MIN	7.97	8.91		2.65	6.79		-0.43	1.38		-0.51	-0.36	
		AVE	9.08	9.00	9.02	7.38	7.41	7.43	1.89	1.91	1.80	-0.17	-0.31	-0.21
	11-Jul-97	MAX	7.93	7.03		7.53	6.80		4.80	0.78		0.71	0.46	
		MIN	5.99	6.84		1.47	5.76		-0.40	-0.09		0.01	0.18	
		AVE	6.90	6.89	6.86	6.50	6.51	6.62	0.10	0.16	-0.02	0.29	0.22	0.25
	15-Jul-97	MAX	9.99	8.96		10.03	7.36		7.01	2.54		0.88	0.60	
		MIN	7.35	8.65		0.75	5.62		-0.56	1.16		0.01	0.26	
		AVE	8.72	8.70	8.66	6.56	6.61	6.59	1.86	1.78	1.81	0.29	0.32	0.25
	20-Jul-97	MAX	9.67	8.70		7.85	7.45		3.97	0.64		1.86	1.34	
		MIN	6.92	8.46		2.92	6.86		0.01	0.21		0.02	0.83	
		AVE	8.55	8.51	8.50	7.16	7.17	7.17	0.50	0.47	0.49	0.89	0.87	0.83

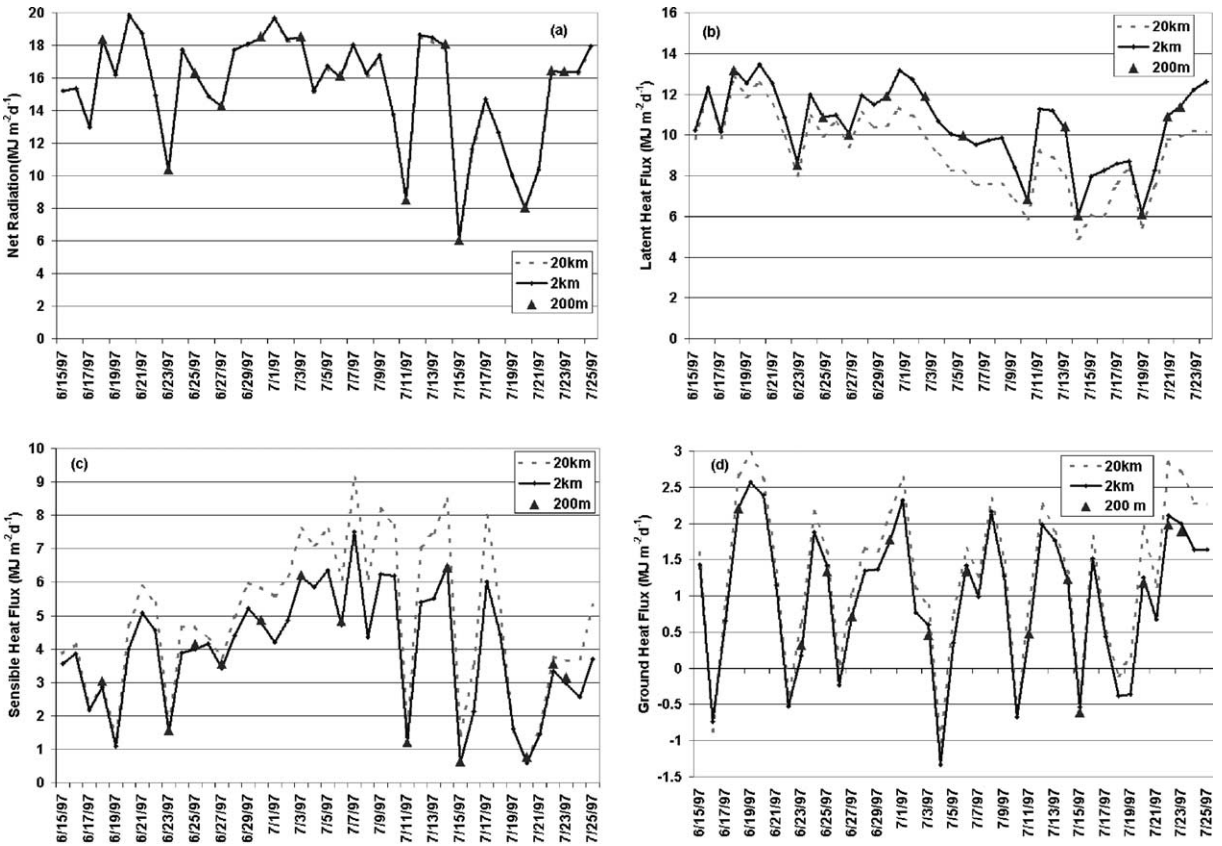

Fig. 10. Scale comparisons of the heterogeneous area (Cell 21) model output at 200-m, 2- and 20-km resolutions.

but in this case it was positive. The patterns for ground heat flux were quite similar to those for sensible heat flux. Thus, energy partitioning at the 20-km scale became biased toward sensible heat and ground heat fluxes, and away from latent heat flux. This trend is consistent with the soil and land use at the 20-km scale for Cell 21. The results confirmed that, for the homogeneous cell, the scaling-up of input data had very little impact on modeled surface energy-balance components. Sridhar et al. (2002) noted that the NOAH LSM overestimated net radiation when evaluated over several sites in Oklahoma, and the mean absolute errors for latent and sensible heat flux combined were greater than those for net radiation. It should be noted that excess energy is allocated predominantly to latent heat flux as opposed to sensible heat flux due to the fact that the latent heat flux is computed first in the model. Modeling inaccuracies due to the aggregation of input data (e.g. at 20 km) could add to the types of flux estimation errors described above. When considering the prediction of late afternoon thunderstorms in mid-latitude regions such as Oklahoma, erroneous computation of fluxes would contribute uncertainty in the estimation of planetary boundary layer thickness and that in turn could result in missing those severe weather activities that are mostly governed by latent heat exchanges on a typical summer day.

Of course, the sub-grid variability which was preserved at the 200-m and 2-km scales becomes non-existent when a single soil type (sand) and single vegetation type (grassland) were assigned for the entire domain of the 20-km resolution analysis. The combination of sand and grassland resulted in reduced latent heat flux at 20 km when compared with the other

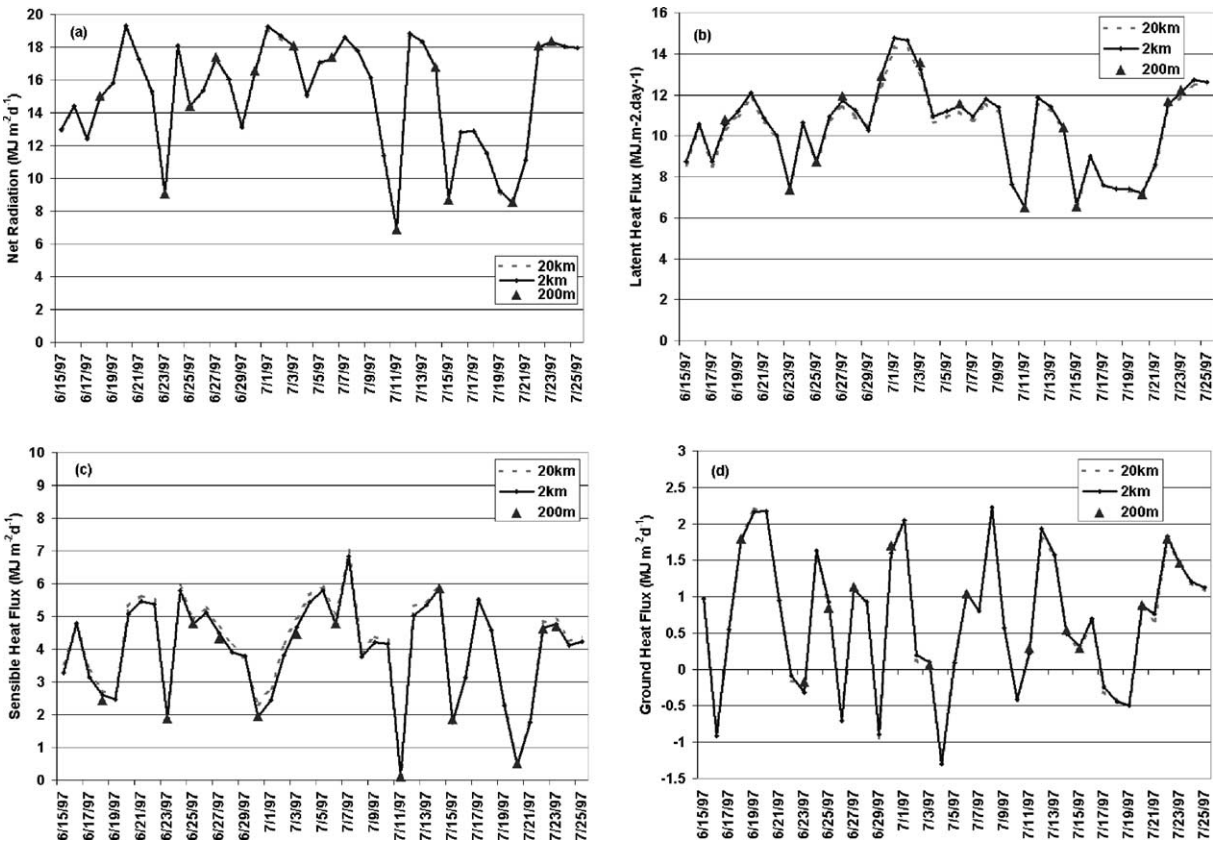

Fig. 11. Scale comparisons of the homogeneous area (Cell 9) model output at 200-m, 2- and 20-km resolutions.

two scales. More of the available energy was then partitioned into sensible and ground heat fluxes. Incorporating 'effective' parameter values could eliminate or at least mitigate the discrepancies introduced at coarser scales, especially over Cell 21. When aggregating the soil type for Cell 21, sand was found to be the dominant soil type while it only accounted for 23% of the total 400 km^2 at 200-m resolution. This resulted in choosing 'end-of-range' values for the physical parameters associated with the sand soil type. However, the other (less 'extreme') soil types in Cell 21 exhibited significantly different parameter values, and a median or weighted average value from the 200-m data would have better represented the overall mix of soil types. Thus, the method of aggregation of input data can certainly impact model results.

Surface fluxes of latent and sensible heat directly influence the evolution and depth of the planetary boundary layer (PBL), and modify its thermodynamic structure. In atmospheric modeling, it would, therefore, be desirable to minimize the bias in predicting latent and sensible heat fluxes. The use of spatially coarse input data can translate into greater uncertainty in tracking PBL phenomena.

6. Summary and conclusions

Large scale modeling of land surface processes is made more complex by sub-grid scale heterogeneity. This research was focused on first identifying the variability in vegetation and soil for the SGP97 region, secondly, on quantifying modeled surface energy-balance components at various spatial scales by aggregating certain input data, and finally on analyzing the scale effects at a sub-grid level for better understanding of land-atmosphere interactions. The well tested NOAH-OSU LSM was used for this study.

Starting with a 280 km × 100 km area in central Oklahoma, a statistical procedure was followed to characterize the variability of soil and vegetation within 70 cells, each 20 km × 20 km. Cell 21 and Cell 9 were identified as the most heterogeneous and the most homogeneous cell, respectively. These areas were found to be heterogeneous and homogeneous in the context of the SGP97 region and not necessarily at regional or continental scales.

The scaling study was performed at 200 m, 2 and 20 km using each of these two cells as a modeling domain. Soil and vegetation input data at the 200-m resolution were aggregated to the coarser scales and model results were analyzed for the following surface energy-balance components: net radiation, latent, sensible and ground heat fluxes.

The domain average net radiation, latent, sensible, and ground heat fluxes estimated for Cell 21 and Cell 9 at 200 m, 2 and 20 km were compared individually. The results indicated that the heterogeneous cell exhibited considerable differences in latent (12% decrease), sensible (22% increase) and ground heat fluxes (44% increase) when soil and vegetation data were aggregated from 200 m to 20 km. The variations in the estimations were insignificant between 200 m and 2 km, however. Though the magnitude of net radiation and thereby other fluxes tended to be less for cloudy days, differences in the estimation of latent and sensible heat fluxes were found to exist between the two coarser scales. As would be expected, Cell 9, the homogeneous cell, responded differently. For both clear and cloudy days, it was evident that the quantification of domain average net radiation, latent, sensible and ground heat fluxes showed no significant difference at the 200-m, 2- and 20-km resolutions.

Improvements in global observing systems and the development and testing of a suite of physically-based LSMs have focused greater attention on identifying the appropriate spatial resolution for modeling efforts. In this particular investigation, the scaling up of high-resolution soil and vegetation input data led to considerable differences in the simulated fluxes over a heterogeneous region. The change in model response occurred between the 2- and 20-km scales; model output for the 200-m scale was very similar to that for the 2-km scale. As expected, scaling-up of input data had very little impact in a relatively homogeneous land area. For the region studied, this analysis concluded that a highly heterogeneous region would require a resolution on the order of 2 km to represent the surface variability for purposes of modeling surface fluxes. The fluxes estimated using 2-km resolution input data are, therefore, expected to reasonably represent the development of any late afternoon mesoscale severe weather events such as thunderstorms, driven mainly by day time heating that are typical over the mid-latitude continental United States. This investigation, besides supporting the argument that sub-grid variability should be considered for proper quantification and partitioning of surface energy-balance components, quantitatively demonstrated the discrepancies in model-simulated fluxes that can result from the scaling up of spatial input data. This is important in improving our understanding on land-atmosphere exchange processes and short term weather forecasting.

Acknowledgements

This research was made possible by EPSCoR grants from the National Aeronautics and Space Administration (Cooperative Agreement Number NCC5-171) and the National Science Foundation (Project Number EPS9550478). The authors also acknowledge the assistance of the Oklahoma Mesonet and the Oklahoma Agricultural Experiment Station. The authors thank Dr Stephen J. Stadler, Department of Geography, Oklahoma State University for helpful discussions on the graphical representation of spatial data.

References

Avissar, R., Pielke, R.A., 1989. A parameterization of heterogeneous land surfaces for atmospheric numerical models and its impact on regional meteorology. Mon. Weather Rev. 117, 2113–2136.

Betts, A.K., Chen, F., Mitchell, K., Janjic, Z.I., 1997. Assessment of the land surface and boundary layer models in two operational versions of the NCEP Eta model using FIFE data. Mon. Weather Rev. 125, 2896–2916.

Brock, F.V., Crawford, K.C., Elliott, R.L., Cuperus, G.W., Stadler, S.J., Johnson, H.L., Eilts, M.D., 1995. The Oklahoma Mesonet: a technical overview. J. Atmos. Ocean Technol. 12 (1), 5–19.

Chen, F., Dudhia, J., 2001. Coupling an advanced land-surface/hydrology model with the Penn State-NCAR MM5 modeling system. Part I. Model implementation and sensitivity. Mon. Weather Rev. 129, 569–585.

Chen, F., Janjic, Z.I., Mitchell, K., 1997. Impact of atmospheric surface-layer parameterization in the new land surface scheme

of the NCEP mesoscale Eta numerical model. Bound.-Layer Meteorol. 85, 391–421.

Chen, F., Mitchell, K., Schaake, J., Xue, Y., Pan, H., Koren, V., Duan, Q.Y., Ek, M., Betts, A., 1996. Modeling of land surface evaporation by four schemes and comparison with FIFE observations. J. Geophys. Res. 101, 7251–7268.

Chen, Z.-Q., Govindaraju, R.S., Kavvas, M.L., 1994a. Spatial averaging of unsaturated flow equations under infiltration conditions over areally heterogeneous fields. 1. Development of models. Water Resour. Res. 30 (2), 523–533.

Chen, Z.-Q., Govindaraju, R.S., Kavvas, M.L., 1994b. Spatial averaging of unsaturated flow equations under infiltration conditions over areally heterogeneous fields. 2. Numerical simulations. Water Resour. Res. 30 (2), 535–548.

DeCoursey, D.G., 1996. Hydrological, climatological and ecological systems scaling: a review of selected literature and comments, Interim Progress Report, USDA-ARS-NPA, Fort Collins, CO

Dooge, J.C.I., 1982. Parameterization of hydrologic processes. In: Eagleson, P.S., (Ed.), Land Surface Processes in Atmospheric General Circulation Models, Cambridge University Press, London, pp. 243–288.

Dooge, J.C.I., 1986. Looking for hydrologic laws. Water Resour. Res. 22 (9), 46S–58S.

Eagleson, P.S., 1978. Climate, soil and vegetation. 1. Introduction to water balance dynamics. Water Resour. Res. 14 (5), 705–712.

Eagleson, P.S., 1986. The emergence of global-scale hydrology. Water Resour. Res. 22 (9), 6S–14S.

Elliott, R.L., Brock, F.V., Stone, M.L., Harp, S.L., 1994. Configuration decisions for an automated weather station network. Appl. Engng Agric. 10 (1), 45–51.

Gutman, G., Ignatov, A., 1998. Derivation of green vegetation fraction from NOAA/AVHRR for use in numerical weather prediction models. Int. J. Remote Sens. 19 (8), 1533–1543.

Henderson-Sellers, A., 1996. Soil moisture: a critical focus for global change studies. Global Planet. Change 13, 3–9.

Hu, Z., Islam, S., 1997. Effects of spatial variabilities on the scaling of land surface parameterizations. Bound.-Layer Meteorol. 83, 441–461.

Jackson, T.J., Le Vine, D.M., Hsu, A.Y., Oldak, A., Starks, P.J., Swift, C.T., Isham, J.D., Haken, M., 1999. Soil moisture mapping at regional scales using microwave radiometry: the Southern great plains hydrology experiment. IEEE Trans. Geosci. Remote Sens. 37 (5), 2136–2151.

Jacquemin, B., Noilhan, J., 1990. Sensitivity study and validation of a land surface parameterization using the HAPEX-MOBILHY dataset. Bound.-Layer Meteorol. 52, 93–134.

Jensen, K.H., Mantoglou, A., 1992. Future of distributed modelling. Hydrol. Process. 6, 255–264.

Kavvas, L.M., 1999. On the coarse-graining of hydrologic processes with increasing scales. J. Hydrol. 217, 191–202.

Kavvas, M.L., Karakas, A., 1996. On the stochastic theory of solute transport by unsteady and steady groundwater flow in heterogeneous aquifers. J. Hydrol. 179, 321–351.

Kavvas, M.L., Chen, Z.Q., Tan, L., Soong, S.-T., Terakawa, A., Yoshitani, J., Fukami, K., 1998. A regional-scale land surface parameterization based on a really-averaged hydrological conservation equations. Hydrol. Sci. J. 43 (4), 611–631.

Koren, V., Schaake, J., Mitchell, K., Duan, Q.-Y., Chen, F., 1999. A parameterization of snowpack and frozen ground intended for NCEP weather and climate model, J. Geophys. Res. 104, 19569–19585.

Koster, R.D., Milly, P.C.D., 1997. The interplay between transpiration and runoff formulations in land surface schemes used with atmospheric models. J. Clim. 10, 1578–1591.

Luxmoore, R.J., King, A.W., Tharp, M.L., 1991. Approaches to scaling up physiologically based soil-plant models in space and time. Tree Physiol. 9, 281–292.

Mahrt, L., Ek, K., 1984. The influence of atmospheric stability on potential evaporation. J. Clim. Appl. Meteor. 23, 222–234.

Mahrt, L., Pan, H.L., 1984. A two-layer model of soil hydrology. Bound.-Layer Meteorol. 29, 1–20.

Marshall Jr., C.H., 1998. Evaluation of the new land-surface and planetary boundary layer parameterization schemes in the NCEP Mesoscale Eta model using Oklahoma Mesonet observations, MS Thesis, University of Oklahoma, Norman, OK, 176 pp

McGarigal, K., Marks, B.J., 1995. FRAGSTATS: spatial pattern analysis program for quantifying landscape structure (version 2.1). Gen.Tech.Rep. PNW-GTR-351. Portland, OR: US Department of Agriculture, Forest Service, Pacific Northwest Research Station, 122 pp

Meentemeyer, V., 1989. Geographical perspectives of space, time and scale. Landscape Ecol. 3, 163–173.

Pan, H.-L., Mahrt, L., 1987. Interaction between soil hydrology and boundary-layer development. Bound.-Layer Meteorol. 38, 185–202.

Robock, A., Schlosser, C.A., Vinnikov, K.Ya., Speranskaya, N.A., Entin, J.K., 1998. Evaluation of AMIP soil moisture simulations. Global Planet. Change 19, 181–208.

Rodriguez-Iturbe, I., Vogel, G.K., Rigon, R., Entekhabi, D., Castelli, F., Rinaldo, A., 1996. On the spatial organization of soil moisture fields. Geophys. Res. Lett. 22 (20), 2757–2760.

Sivapalan, M., Woods, R.A., 1995. Evaluation of the effects of general circulation models' subgrid variability and patchiness of rainfall and soil moisture on land surface water balance fluxes. In: Kalma, J.D., Sivapalan, M. (Eds.), Scale Issues in Hydrological Modeling, Wiley, England, pp. 453–473.

Southern Great Plains 1997 (SGP 97) hydrology experimental plan, 1997. USDA Agricultural Research Service, Beltsville, MD, 178 pp

Sridhar, V., Elliott, R.L., 2002. On the development of a simple downwelling longwave radiation scheme. Agric. Forest Meteorol. 112, 237–243.

Sridhar, V., Elliott, R.L., Chen, F., Brotzge, J.A., 2002. Validation of the NOAH-OSU Land surface model using surface flux measurements in Oklahoma. J. Geophys. Res. 107 (D20), 4418doi:10.1029/2001JD001306.

Wood, E.F., 1994. Scaling, soil moisture and evapotranspiration in runoff models. Adv. Water Resour. 17, 25–34.

Wood, E.F., Lettenmaier, D.P., Zartarian, V.G., 1992. A land-surface hydrology parameterization with subgrid variability for general circulation models. J. Geophys. Res. 97, 2717–2728.

Yucel, I., Shuttleworth, W.J., Washburne, J., Chen, F., 1998. Evaluating NCEP Eta model derived data against observations. Mon. Weather Rev. 126, 1977–1991.